SOA pattern effect mitigation by neural network based pre-equalizer for 50G PON

N.B. When citing this work, cite the original published paper.

(article starts on next page)

SOA pattern effect mitigation by neural network based pre-equalizer for 50G PON

Lei Xue,[1,2] **Lilin Yi,**[1,*] **Rui Lin,**[2] **Luyao Huang,**[1] **and Jiajia Chen**[2]

[1]*State Key Laboratory of Advanced Optical Communication Systems and Networks, Shanghai Jiao Tong University, Shanghai 200240, China*
[2]*Chalmers University of Technology, S-412 96 Göteborg, Sweden*
[*]*lilinyi@sjtu.edu.cn*

Abstract: Semiconductor optical amplifier (SOA) is widely used for power amplification in O-band, particularly for passive optical networks (PONs) which can greatly benefit its advantages of simple structure, low power consumption and integrability with photonics circuits. However, the annoying nonlinear pattern effect degrades system performance when the SOA is needed as a pre-amplifier in PONs. Conventional solutions for pattern effect mitigation are either based on optical filtering or gain clamping. They are not simple or sufficiently flexible for practical deployment. Neural network (NN) has been demonstrated for impairment compensation in optical communications thanks to its powerful nonlinear fitting ability. In this paper, for the first time, NN-based equalizer is proposed to mitigate the SOA pattern effect for 50G PON with intensity modulation and direct detection. The experimental results confirm that the NN-based equalizer can effectively mitigate the SOA nonlinear pattern effect and significantly improve the dynamic range of receiver, achieving 29-dB power budget with the FEC limit at $1e^{-2}$. Moreover, the well-trained NN model in the receiver side can be directly placed at the transmitter in the optical line terminal to pre-equalize the signal for transmission so as to simplify digital signal processing in the optical network unit.

1. Introduction

The explosive bandwidth consuming services, like virtual reality (VR), 8K videos, and cloud services drive capacity upgrade of the access network to satisfy ever-increasing users' demand. Passive optical network (PON) has been demonstrated to be the most promising and cost-effective broadband access technology. During the past two decades, the line rate of PON increased from 1G to 10G, and 25G. The international standardization ITU Q2/SG15, and IEEE 802.3ca task force started to standardize 50G per wavelength in recent years [1–2]. Many research works show their solutions for 50G [3–4] or even 100G [5–6] PON. Among these solutions, intensity modulation and direct detection (IMDD) is chosen as the mainstream technique due to its simplicity and low cost compared to coherent detection. Since high-speed signal are sensitive to fiber dispersion, O-band is selected as the working waveband for 100G PON [7] at the expense of a higher insertion loss of 0.33 dB/km, which on the other hand would put more pressures on the system power budget. Avalanche photodiode (APD) with high receiver sensitivity is considered as the receiver in the optical network unit (ONU) to ensure enough power budget for downstream. The commercial APD with big volume is 10G-class, and nowadays the 25G-class APD is still costly. An alternative choice is combining the photodiode (PD) with the semiconductor optical amplifier (SOA). The high-bandwidth PD is already mature for 100G large-scale Ethernet applications. Moreover, compared with the APD, the PD is usually with better linear response which is more suitable for high-order modulation formats. Meanwhile, the SOA works as a pre-amplifier to increase the signal power injected into the PD. Therefore, the receiver sensitivity can be greatly improved. However, the nonlinear pattern effect due to

the SOA gain saturation degrades performance, particularly for high-speed signal [8]. Several approaches have been proved to be effective in the mitigation of SOA nonlinearity [9–11]. In [9] SOA induced frequency shift needs to be considered when applying optical filter after the SOA. The approach introduced in [10] requires an extra wavelength for the gain-clamped SOA. Digital backpropagation approach [11] brings high complexity to the receiver at the ONU side. The lack of flexibility and high complexity introduced at the ONU hinder their applications in high-speed PONs.

Neural network (NN) has been demonstrated to be a powerful tool to compensate linear and nonlinear impairments in optical transmission system and outperforms some conventional digital signal processing (DSP) algorithms, e.g., feed forward equalizer (FFE) and Volterra [12–13]. However, NN is mainly deployed at the receiver side. If directly employing it in the PON, the high computation complexity introduced at the receiver of the ONU makes it difficult for real deployment. Even though some pruning algorithms can simplify the NN structure [14], it would be more beneficial to employ NN at the transmitter of the optical line terminal (OLT), where all connected ONUs can share the deployment cost.

In this paper, for the first time, we propose to use a well-trained NN-based pre-equalizer to mitigate SOA pattern effect in a 50G PON system with IMDD. Thanks to the capability of nonlinearity compensation, the pattern effect induced dynamic range limitation can be significantly improved by the NN. By introducing training data from multiple sampling, the NN model shows better performance resisting system dynamics. Moreover, placing the well-trained NN model generated from the ONU at the OLT for pre-equalization significantly reduces the deployment cost of the ONU while maintaining performance for nonlinearity mitigation.

2. SOA nonlinear pattern effect

The SOA gain G, is defined as the ratio between output power and input power P_{in}. With the increase of P_{in}, carriers inside the SOA active $G = G_0 e^{\left(-\frac{G-1}{G}\right)*\frac{P_{out}}{P_{sat}}}$ region deplete, rP_{out} esulting in gain saturation [15]. The relationship between G and P_{out} can be expressed as follow:

$$G = G_0 e^{\left(-\frac{G-1}{G}\right)*\frac{P_{out}}{P_{sat}}}, \tag{1}$$

where G_0 is the small signal gain, and P_{sat} is the saturation power defined as the output power at which G_0 is compressed by 3 dB. P_{sat} is the boundary between linear and nonlinear region. When $P_{in} \ll P_{sat}$, $\left(-\frac{G-1}{G}\right)*\frac{P_{out}}{P_{sat}} = (1-G)*\frac{P_{in}}{P_{sat}}$, gets close to 0, then we can get $G \cong G_0$ and the SOA works in linear amplification mode. As the increase of P_{in}, G decays exponentially. Figure 1 shows the measured curve of the SOA used in this experiment. The SOA saturation output $G - P_{out}$ power is 7 dBm and it begins to saturate when the input power is higher than -13 dBm.

After signal modulation, G becomes time-variant since the instantaneous power of input pulse varies with time. In this case, the SOA instantaneous gain $G(t)$ [15] can be expressed as:

$$G(t) = \frac{G_0}{G_0 - (G_0 - 1)e^{(-E(t)/E_s)}}. \tag{2}$$

$E(t)$ represents the fraction energy of input pulse contained in the leading part of pulse up to $\tau < t$, which can be expressed as:

$$E(t) = \int_{-\infty}^{t} P_{in}(\tau)d_\tau. \tag{3}$$

In (2), E_s is the saturation energy. For a single pulse with energy $E_g > E_s$, with the leading-edge gain $G(-\infty) = G_0$, the SOA is not saturated, while for the trailing-edge, the gain $G(\infty) = G_0/[G_0 - (G_0 - 1)e^{(-E_g/E_s)}]$. Therefore, the pulse shape evolves from rectangle to jagged waveform and the gain compression becomes more serious for input pulse with higher power.
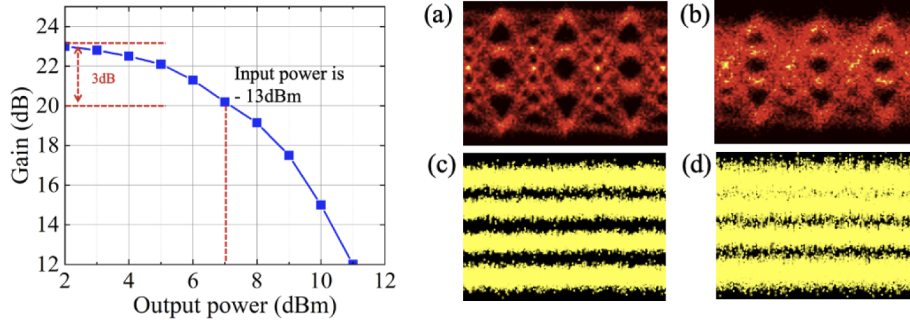
Fig. 1. The measured SOA gain as a function of output power. Insets (a) and (b): eye diagrams without and with SOA pattern effect; Insets (c) and (d): PAM-4 signal symbols without and with SOA pattern effect.

Moreover, for a series of data, the former symbol also influences SOA gain to the current symbol, which is known as the pattern effect. Taking 4-level pulse amplitude modulation (PAM-4) as an example, the insets (a)-(d) of Fig. 1 show the eye diagrams and symbol levels without and with such SOA pattern effect, where the input power is -18 dBm and -5 dBm, respectively. It is clear that the eye diagram is distorted by the pattern effect and more severe distortion is observed on higher levels of the PAM-4 signal.

3. Principle of NN based pre-equalizer and offline DSP flow

3.1. NN based pre-equalizer

Figure 2 shows the architecture of NN based pre-equalizer. The target function of this architecture can be written as follows: x

$$
\hat{\Theta} = arg\,\min_{\Theta} ||d(n)|| = arg\,\min_{\Theta} ||u(n) - u'(n)||
$$
$$
= H_{NN}[x(n), \theta] - H_{NN}[y(n)/G, \theta] \tag{4}
$$

where $u(n)$ and $u'(n)$ are the output signal from pre-NN and post-NN, H_{NN} denotes the function of pre- and post-NN. If the network is trained perfectly, we can consider the error $d(n) = 0$, then

$$
H_{NN}[x(n), \theta] = H_{NN}[y(n)/G, \theta] \tag{5}
$$

and consequently,

$$
y(n) = Gx(n) \tag{6}
$$

where G is the scaling factor.

Typically, $d(n)$ does not vanish completely because the NN model may not be estimated perfectly. Moreover, the SOA presents a time-varying response, even the well-trained network at the receiver side may not be perfect when applied at the transmitter side. To relieve this effect, the post-NN model is trained by a double-sized training data sampled at two time slots aiming at learning SOA dynamic features. From above deductions, the normalization gain G should be properly set for a unit gain provided by the NN. In this case, the values of received signal are normalized to -3 to 3 before training in the NN. By employing double-sized training data samples and normalization, the swap of the NN from post- to pre-equalizer can work efficiently.

3.2. DSP flow

The DSP block at the transmitter side (Tx) is shown in green in Fig. 3(a). Random data generated by Mersenne twister are mapped into PAM-4 symbols with a length of 2^{15}. To compensate the
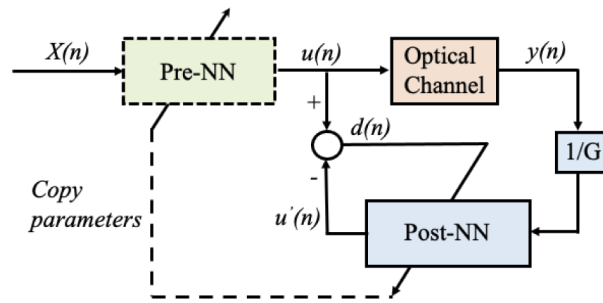
Fig. 2. Architecture of NN based pre-equalizer.

bandwidth limitation from the optoelectrical devices, time-domain digital pre-emphasis based on linear finite impulse response (FIR) filter and Nyquist pulse shaping based on root-raised-cosine (RRC) filter with the optimal roll-off factor 0.15 are used to reduce the corresponding inter-symbol interference (ISI) effect. The FIR filter is estimated from the FFE under the back-to-back (BtB) case. The spectra before and after RRC is shown in Fig. 3(b) and (c), respectively. Next, the symbol sequence is resampled to match the sampling rate of the arbitrary waveform generator (AWG).
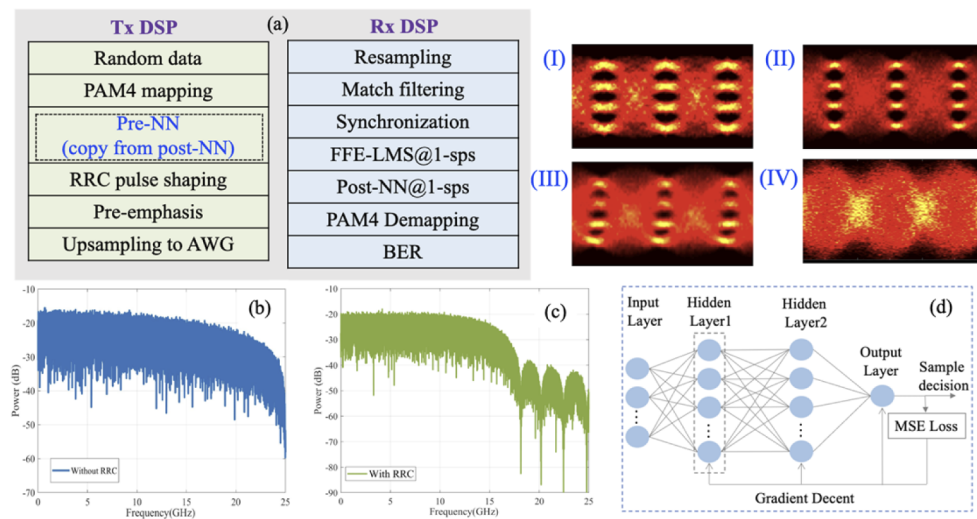

Fig. 3. (a) The offline DSP blocks at Tx and Rx side, (b) and (c) transmitted spectra of original PAM-4 before and after RRC, respectively, and (d) NN structure. Insets are the electrical eye diagram of 25Gbaud PAM-4: (I) and (II) with RRC and the roll-off factor is 0.4 and 0.15 respectively, (III) with pre-NN equalization, and (IV) with pre-emphasis.

The offline DSP block at the receiver side (Rx) is shown in blue in Fig. 3(a). The captured offline data is first resampled to 1-sample per sequence (sps) with the matched filter, and then synchronization is applied to remove the time jitter and extract the sending data. Afterwards, a FFE filter is followed to pre-converge the data which can accelerate the convergence of the post-NN in the next stage. Once the post-NN converged, then it is transferred to the Tx side for pre-equalization and only the FFE is employed at the Rx side. The electrical eye diagrams of 25Gbaud PAM-4 signal with Tx DSP are shown in Insets (I) to (IV), respectively. It can be

observed that the eye diagram after pre-NN is distorted since the NN with a reverse nonlinear response of SOA.

The training data set for NN is sampled with received optical power of 0 dBm when strong pattern effect appears. The structure of the NN-based equalizer is shown in Fig. 3(d). It is a 4-layer fully connected network, containing input layer, two hidden layers and output layer. The input layer has 107 nodes, which means 107 consecutive sampled symbols are required as input for one symbol decision. Each hidden layer has 48 nodes, while the output layer has 1 node. The activation function of hidden layers is ReLU and the optimal learning rate is set as 0.0001. The training is carried out with the optimization technique Adam [5]. The size of the whole data set is 100,000, with 50,000 symbols for training and 50,000 symbols for the final test. The final bit-error rate (BER) performance is evaluated based on the test data set.

4. Experimental setup and result discussion

4.1. Experimental setup

The experimental setup is shown in Fig. 4. At the transmitter side, the 25Gbaud PAM-4 signal is generated by an arbitrary waveform generator (AWG, Keysight 8195A) working at 65 GSa/s with the 3-dB analog bandwidth of 20 GHz. The output signal is first amplified to 1.8 Vpp by an electrical amplifier (EA) before driving the commercial 20 Gbps directly modulated laser (DML) with a 3-dB bandwidth of 12 GHz and a center wavelength of 1315 nm. The end-to-end frequency response and the spectra before and after modulation are shown in Insets (a) and (b) of Fig. 4. Then, the 25Gbaud PAM-4 optical signals are transmitted over 20 km standard single mode fiber (SSMF) with an average loss of 0.33 dB/km at 1310 nm. An O-band polarization independent SOA (Inphenix IPSD 1316c) with a noise figure of 7 dB is used at the receiver side before direct detection. A variable optical attenuator (VOA) is applied to emulate the splitter loss and also test the SOA performance. The measured OSNR of 25Gbaud PAM-4 signals after SOA is shown in Inset (c) of Fig. 4, where the SOA bias current is optimized to 250 mA. Higher bias current generates more amplified spontaneous emission (ASE) noise. Note that the optical filter in our lab with 6-dB insertion loss cannot further improve the receiver sensitivity, so it is not used after the SOA for filtering ASE noise. A 40G PD is used to convert the optical signal to electrical signal. Following the PD, the output signal is captured by a 40 GSa/s oscilloscope with 20 GHz bandwidth and processed by the offline DSP.

4.2. Experimental results and discussion

To understand how the NN works, we start from the BtB case and first measure the eye diagram of 25Gbaud PAM-4 signal directly detected by a PD without SOA for pre-amplification. The results are shown in Fig. 5. The eye diagrams are clearly open since there is no nonlinear distortion (see Fig. 5(a)). After employing SOA as a pre-amplifier, the pattern effect due to the gain saturation degrades the signal quality. As explained in Section 2, the SOA gain decreases as the input power increases, and the higher levels of the PAM-4 signal corresponding to higher optical power are amplified with lower gain. From the histogram of Fig. 5(b), it can be observed that levels '1' and '3' are aliased between each other resulting closed eye diagram. To compensate the nonlinear distortion, a fully connected NN is employed as nonlinear equalizer at the receiver side to recover the signal. It can be seen from Fig. 5(c), the more aliasing at the higher levels is mitigated, so a clearer eye diagram and a higher peak in the histogram can be observed. However, applying the NN as a post-equalizer in the ONU increases the complexity and deployment cost. Based on the analysis in Section 3.1, we can move the well-trained NN module to the OLT side as a pre-equalizer, allowing for sharing DSP complexity by all the connected ONUs and thus lowering operation and deployment cost.
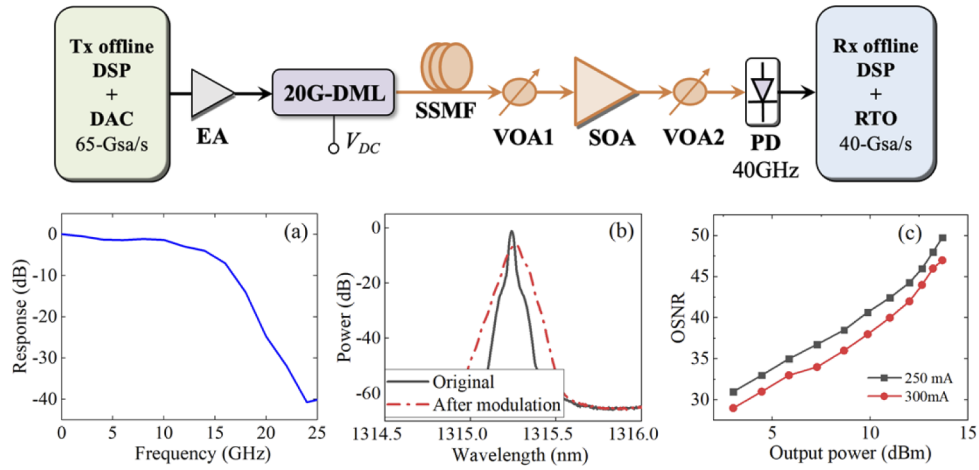
Fig. 4. Experimental setup of 50 Gb/s/λ PAM-4 PON; Insets: (a) Frequency response of end-to-end system, (b) optical spectra of signal and (c) measured OSNR of 50Gb/s PAM-4 signal versus SOA output power.
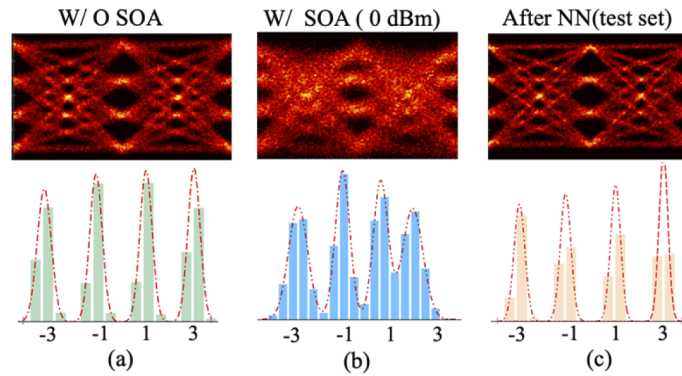

Fig. 5. Eye diagrams and histograms of 25Gbaud PAM-4 signal for the BtB tests: (a) without SOA, (b) with SOA, and (c) with SOA after the post-NN equalizer.

In the practical deployment, the SOA features can be learned in the lab. Once the well-trained NN is obtained, it can be directly applied at the OLT side without additional manipulation in the ONU to adapt to nonlinear dynamics induced by the SOA. Note that since O-band is employed here, the dispersion induced performance variations due to different distance to the OLT is minor and can be neglected. Otherwise, to mitigate such dispersion induced performance variations the NN should be trained with data from different distances and wavelengths achieving a universal NN [16].

Figure 6(a) shows the BER performance comparison between NN-based post- and pre-equalizer. Both of them can achieve around -21 dBm sensitivity at the low-density parity-check forward error correction (LDPC) FEC limit of 1×10^{-2} [17]. However, if the NN model is trained with data sampled at just one time slot, the pattern effect cannot be well compensated when the SOA has high input power. The performance gap mainly comes from the time-varying feature of the SOA as mentioned earlier. After training with double-sized data sampled at two time slots, the BER gap is reduced.

To evaluate the system performance of using the SOA as a pre-amplifier, we first measure and compare the receiver sensitivity before and after using the SOA. The results are shown in
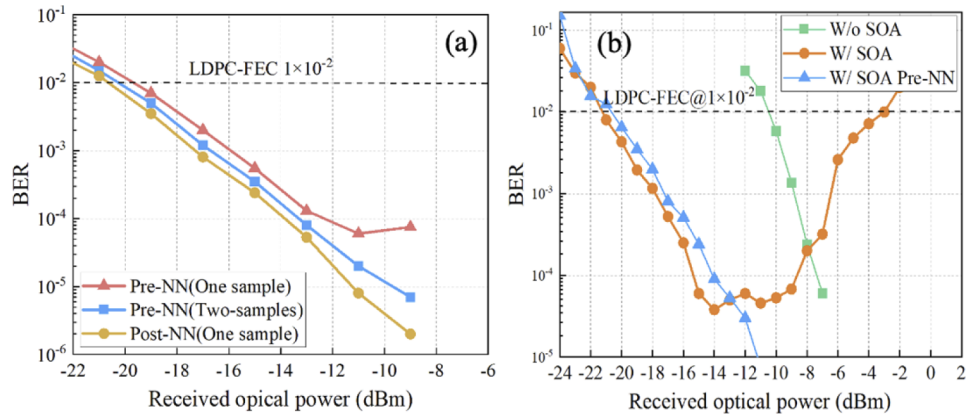
Fig. 6. BER of 25Gbaud PAM-4 signals: (a) performance comparison between NN-based pre-equalizer and post-equalizer at the back-to-back test. (b) with 20 km SSMF at O-band with and without SOA.

Fig. 6(b). Without the SOA, the optical signal is directly injected into the PD for detection. The sampled signal is processed offline by a 37-tap FFE, and the receiver sensitivity of -10 dBm is achieved. After employing the SOA as pre-amplifier, 10 dB improvement can be obtained at the LDPC FEC limit. However, the BER curve changes with the input power. In the beginning, the BER drops rapidly with the increase of the received optical power thanks to the improved optical signal-to-noise ratio (OSNR). When the input power is higher than -14 dBm, the SOA is saturated and the BER stops decreasing due to nonlinear pattern effect even given a higher OSNR. When the input power surpasses -8 dBm, degraded BER performance can be observed, which can be attributed to the worse nonlinear effect. The dynamic range of receiver is an important performance indicator for the receivers deployed in PON. Considering the BER at 1×10^{-2}, a dynamic range is limited to 18 dB when the SOA is employed. To enlarge the dynamic range of the receiver, nonlinear effect needs to be compensated. Following the previous analysis, the NN is first trained by 100,000 sampled at the receiver side and then applied to the transmitter side for pre-equalization. As shown in Fig. 6(b), the BER decreases continually with the increase of the
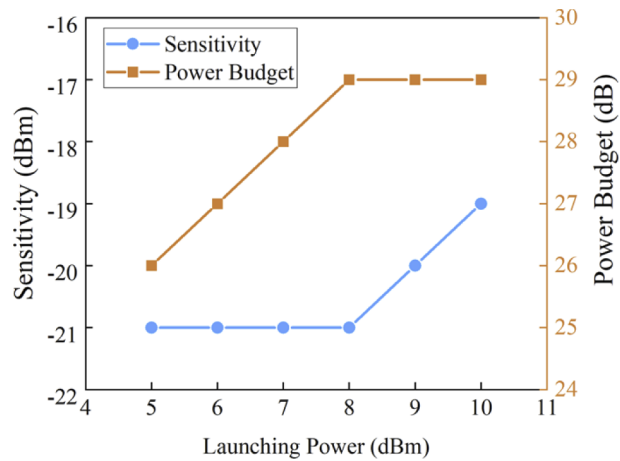

Fig. 7. Receiver sensitivity and system power budget versus the DML launching power.

received optical power. When the power is higher than -10 dBm, the BER is lower than 1×10^{-5} which cannot be displayed, indicating a significantly improved dynamic range of the receiver. Note that there is no optical filter used between the SOA and PD in the experiment, therefore the SOA + PD solution is easy for integration as a high-sensitivity receiver with low cost.

Finally, we evaluate the system power budget and receiver sensitivity at different launching power for 25Gbaud PAM-4 PON (i.e., 50G PON). As shown in Fig. 7, the optimal launching power of the DML is 8 dBm and the corresponding power budget can reach 29 dB which is able to meet the PR-30 requirement [18]. Higher launch power makes the DML bias at nonlinear range causing nonlinear distortion, and the receiver sensitivity turns to be degraded accordingly.

5. Conclusion

We have proposed to use the NN-based pre-equalizer at the OLT to compensate the nonlinear pattern effect in the high-speed PON system where the SOA + PD is employed as a low-cost optical receiver at the ONU. A data set taking multiple sampling is employed for training a NN model which is adaptive to system dynamics. Applying the equalizer at the transmitter side can relax the complexity of DSP needed at each ONU and allows for sharing the cost with all ONUs while maintaining system performance. The experiment validation reveals that the NN-based pre-equalizer effectively compensate the SOA nonlinear patten effect, improving the dynamic range of the receiver and offering a power budget as high as 29 dB for the 50G PON system.

Disclosures. The authors declare no conflicts of interest.

Data availability. Data underlying the results presented in this paper are not publicly available at this time but may be obtained from the authors upon reasonable request.

References

1. D. Nesset, "PON roadmap [invited]," J. Opt. Commun. Netw. **9**(1), A71–A76 (2017).
2. G.989 series of ITU specifications, https://www.itu.int/rec/T-REC-G/en.
3. C. Li, J. Chen, Z. Li, Y. Song, Y. Li, and Q. Zhang, "Demonstration of symmetrical 50-Gb/s TDM-PON in O-band supporting over 33-dB link budget with OLT-side amplification," Opt. Express **27**(13), 18343–18350 (2019).
4. M. S. Erkılınç, D. Lavery, P. Bayvel, R. I. Killey, S. J. Savory, and C. Schubert, "Coherent ONU designs for 50Gb/s/λ PON," in *Optical Fiber Communications Conference (OFC)* (2019), paper Th3F.5
5. L. Yi, T. Liao, L. Huang, L. Xue, P. Li, and W. Hu, "Machine learning for 100 Gb/s/λ/ passive optical network," J. Lightwave Technol. **37**(6), 1621–1630 (2019).
6. J. Zhang, J. Jun, X. Li, Y. Wei, K. Wang, L. Zhao, W. Zhou, M. Kong, X. Pan, B. Liu, and X. Xin, "100 Gbit/s VSB-PAM-n IM/DD transmission system based on 10 GHz DML with optical filtering and joint nonlinear equalization," Opt. Express **27**(5), 6098–6105 (2019).
7. E. Harstead and J. Johnson, "25G and 50G EPON downstream wavelength plan," *5 March 2018 IEEE 802.3 Plenary*, Chicago, IL, USA.
8. K. Wang, J. Zhang, L. Zhao, X. Li, and J. Yu, "Mitigation of Pattern-Dependent Effect in SOA at O-Band by Using DSP," J. Lightwave Technol. **38**(3), 590–597 (2020).
9. Z. Rizou, K. Zoiros, and A. Hatziefremindis, "Comparison of Basic Notch Filters for Semiconductor Optical Amplifier Pattern Effect Mitigation," Appl. Sci. **7**(8), 783 (2017).
10. K. Taguchi, H. Nakamura, K. Asaka, T. Mizuno, Y. Hashizume, and T. Yamada, "40-km Reach Symmetric 40-Gbit/s tunable WDM/TDM-PON Using Synchronized Gain-Clamping SOA," in *Optical Fiber Communications Conference (OFC)* (2013), paper OW4D.6.
11. A. Ghazisaeidi and L. A. Rusch, "On the Efficiency of Digital Back-Propagation for Mitigating SOA-Induced Nonlinear Impairments," J. Lightwave Technol. **29**(21), 3331–3339 (2011).
12. A. G. Reza and J. K. K. Rhee, "Nonlinear Equalizer Based on Neural Networks for PAM-4 Signal Transmission Using DML," IEEE Photonics Technol. Lett. **30**(15), 1416–1419 (2018).
13. M. Luo, F. Gao, X. Li, Z. He, and S. Fu, "Transmission of 4×50-Gb/s PAM-4 Signal over 80-km Single Mode Fiber using Neural Network," in *Optical Fiber Communications Conference (OFC)* (2018), paper M2F.2.
14. Z. Wan, J. Li, L. Shu, M. Luo, X. Li, S. Fu, and K. Xu, "Nonlinear equalization based on pruned artificial neural networks for 112-Gb/s SSB-PAM4 transmission over 80-km SSMF," Opt. Express **26**(8), 10631–10642 (2018).
15. G. P. Agrawal and N. A. Olsson, "Self-phase modulation and spectral broadening of optical pulses in semiconductor laser amplifiers," IEEE J. Quantum Electron. **25**(11), 2297–2306 (1989).
16. V. Houtsma, E. Chou, and D. Van Veen, "92 and 50 Gbps TDM-PON using Neural Network Enabled Receiver Equalization Specialized for PON," in *Optical Fiber Communications Conference (OFC)* (2019), paper M2B.6.

17. IEEE P802.3ca 50G-EPON Task Force, "Physical layer specifications and management parameters for 25 Gb/s and 50 Gb/s passive optical networks," http://www.ieee802.org/3/ca/index.shtml.

18. V. Houtsma, D. Veen, and E. Harstead, "Strategies for economical next-generation 50G and 100G passive optical networks," J. Opt. Commun. Netw. **12**(1), A95–A103 (2020).